

Small- and Full-Scale Fatigue Testing of Lead Cable Sheathing

Audun Johanson¹, Luigi Mario Viespoli², Antonio Alvaro³, Filippo Berto²

¹Nexans Norway,

²Dept. Of Mechanical and Industrial Engineering, Norwegian University of Science and Technology (NTNU), Norway

³Dept. of Materials and Nanotechnology, SINTEF Industry, Norway

ABSTRACT

The fatigue behavior of a PbSnSb alloy used in subsea power cable sheathing was studied using small- and full-scale experiments. The aim of the work was to understand the transferability between the scales and suitable testing methods. Creep phenomena are addressed by considering the cyclic strain rate as well as the small-scale loading mode. The fatigue test results show significant difference between different loading modes and scales. It is also evident that fatigue- creep interaction is highly important.

KEY WORDS: Lead Sheath; Fatigue; Creep; Subsea Power Cables.

INTRODUCTION

Subsea power cables operating above 36 kV require an impermeable water barrier to prevent humidity in the isolation system. In the case of Mass-Impregnated (MI) or Cross-Linked High Density Polyethylene (XLPE) insulation systems as normally used for high voltage submarine power cables, humidity can compromise the systems electrical integrity. Lead-based alloys are normally used as a water barrier due to ease of extrudability and ductility. Lead-based alloys are also associated with favorable low-cycle fatigue properties when compared to higher strength materials such as copper or aluminum. However, due to its combination of very poor high cycle fatigue properties and low creep resistance, multiple cyclic scenarios can challenge the fatigue-creep life of the sheathing. Critical scenarios include cable installation and offshore jointing. These operations imply a temporary dynamic suspension between the seabed and a floating vessel where the cable will be subjected to bending due to wave motion on the cable and vessel. Additional bending fatigue damage can be introduced from vortex-induced vibrations (VIV) in the temporary catenary or free-spans along the cable route. Another case arises from the insulation temperature fluctuations during operation. Thermal expansion and contraction of the oil in MI insulation or the XLPE will cyclically strain the lead sheath in radial direction. The high relative temperature for lead-alloys at room temperature ($\sim 0.5 T_m$) and low creep resistance for typical cable sheathing alloys cause a significant strain rate dependency under loading. These properties also depend on the alloying elements and the microstructure.

The fatigue performance of a Lead-Tin- Antimony (PbSnSb) - alloy as

cable sheathing on MI- and XLPE power cables have been investigated. The alloy is common in the subsea power cable industry, but its fatigue and creep properties, probably due to the numerous challenges inherent to testing and metallurgical investigation, have been subject to limited research. The existing literature, which is quite scarce, include the work of Anelli (1986) who investigated the frequency dependency of the alloy. In a recent publication by the authors, the importance of microstructure of this alloy with respect to its strain rate dependency at room temperature (Viespoli et al., 2019).

In this work cyclic fatigue testing on both small- and component/full-scale level have been conducted. The material has been subjected to two different loading modes: reverse bending and tension- compression. Particular attention is payed to the influence of creep by considering the strain rate sensitivity.

MATERIALS AND METHODS

Materials and Test Specimens

This study investigates an extruded PbSnSb alloy with composition given in Table 1. The as-extruded grain size is approximately 70 μm by the average grain intercept method.

Table 1. Composition of test material.

Pb	Sn	Sb
99.3	0.45	0.25

Four types -of test specimens have been investigated in this study:

- (1) 3.0 mm thickness as- extruded 3.0 mm rectangular specimens for reverse bending;
- (2) 3.0 mm thickness as- extruded rounded hourglass shaped specimens tension- compression tests;
- (3) MI full scale power cable;
- (4) XLPE power phases.

Figure 1 show the MI power cable and XLPE power phase cross-sections.

Small Scale Test Procedures

Reverse Bending. Cyclic reverse bending testing has been carried out to investigate the fatigue life under such loading mode and effect of strain rate.

Forty four reverse bending tests over 11 different test parameters have

been performed (the test parameters are summarized in Table 2). The test object target strain range ($\Delta\epsilon$) is controlled by fixing the test object horizontally and vertically displacing it against a shaper with a defined curvature (Figure 2).

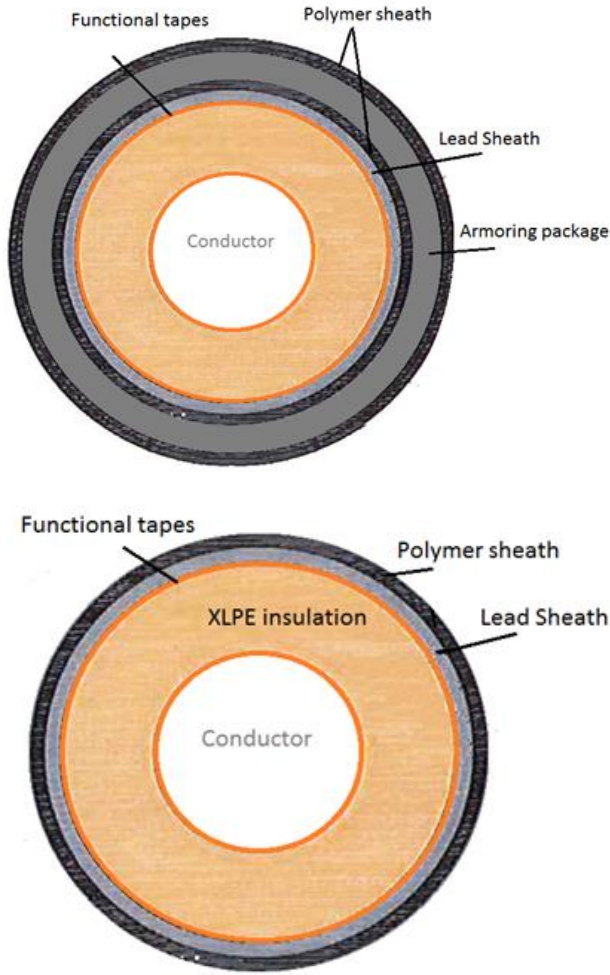


Fig. 1. (Upper) MI power cable test object; (Lower) XLPE power phase test object. A XLPE power cable often consists of 3 XLPE power phases stranded together where axial armoring is applied on the outside of the 3-phase cross-section. Functional tapes indicate one or more layers of helically wound tapes for various purposes.

The strain range is calculated according to Eq. 1.

$$\Delta\epsilon_{nom} = C_{Shaper} t_{test\ Object} \quad (1)$$

Where C and t are the measured curvature and thickness of each individual test object, respectively.

Failure is measured by electrical resistance of each samples whereby an increase is caused by fracture and separation of the specimen. All tests are conducted at room temperature.

Tension-compression. Cyclic loading testing in tension-compression has been conducted to investigate the fatigue life under such loading mode.

Eight tests at different $\Delta\epsilon$ and constant strain rate (i.e. $1e-2$ 1/s), were carried out. Triangular shaped load cycles were used in order to assure a

strain rate as constant as possible for the duration of the whole test. The strain rate value was chosen with the intent of excluding creep and thus strain rate dependency (Viespoli, et al., 2019).

Table 2. Test matrix. Four tests for each parameter parallel.

Shaper curvature [1/m]	$\Delta\epsilon$ (nom.)	Frequency [Hz]
1.00	0.32 %	1
		$3.3e^{-1}$
		$1.7e^{-2}$
		$2.8e^{-3}$
		$8.3e^{-3}$
0.67	0.21 %	1
0.50	0.16 %	$1.3e^{-1}$
		2
		1
		$3.5e^{-1}$
		$1.3e^{-1}$

Symmetric loading ($R = -1$) is employed for all tests where and the strain is measured by Digital Image Correlation (DIC) technique.

The test set-up is shown in Figure 3.

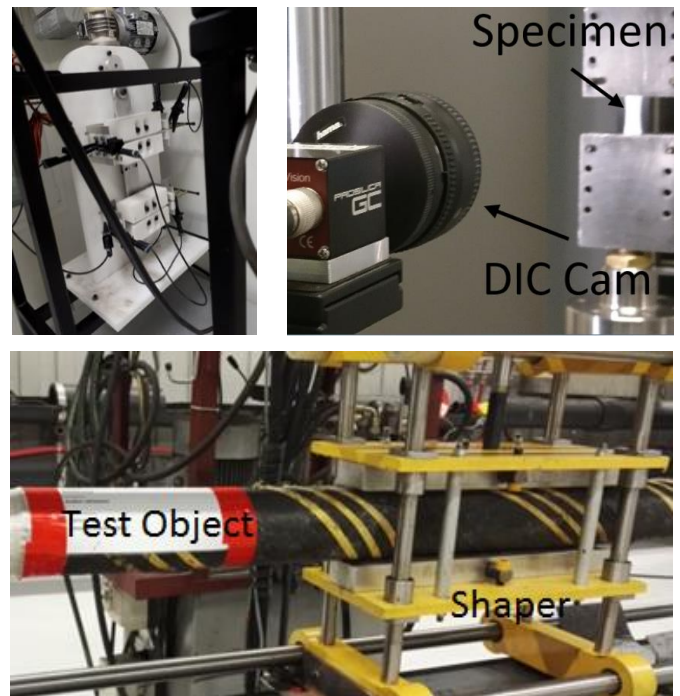


Fig. 3. (Upper Left) Cyclic reverse bending set-up; (Upper Right) Tension- Compression set up and DIC strain measurement; (Lower) Full scale test set-up.

Full Scale Test Procedure

In total 27 XLPE power phases and 30 MI power cable test object were subjected to reverse bending. The set-up is shown in Figure 2. The test objects are tensioned to 5 kN in order to straighten the test object prior and during the test. 600 mm long shapers of defined curvatures are mounted with its curved side facing the test object from each side. The

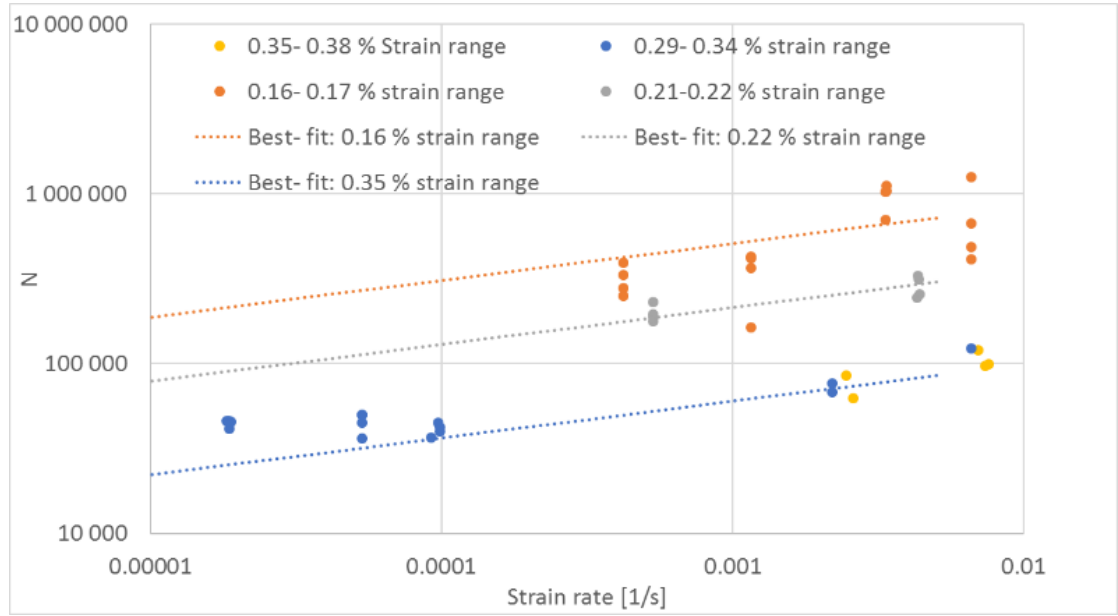


Fig. 3. Reverse bending fatigue results and best-fit fatigue-creep model. The damage model appears to over-predict the creep damage towards low strain rates, at which it results too conservative.

test object is bent by displacing the shapers vertically until the test object is in contact with the shaper over 400- 500 mm at its minimum and maximum positions. The vertical shaper displacement amplitude is kept constant throughout the test.

The strain range is calculated from the measured test object sheathing diameter and radius of the shapers according to Eq. 1 where t is the test object diameter.

Test temperature is maintained at room temperature.

Due to the lack of a reliable failure detection system, all tests are run to a pre- specified number of cycles where post- test dissection and die-pen investigation of the lead surface is used to determine if the test object had failed.

The test matrix is given in Table 3.

Table 3. Test matrix. In total 30 MI full scale power cables and 27 XLPE power phases where tested.

Shaper curvature [1/m]	Test Object/ OD [mm]	$\Delta\varepsilon$ (nom.)	Frequency [Hz]
0.110	MI/ 95.8	1.02 %	0.20
	MI/ 66	0.70 %	0.10
	XLPE/ 105.6/	1.11 %	0.20
0.037	MI/ 95.8	0.36 %	0.20, 0.33, 0.44
	MI/ 66	0.24 %	0.25
	XLPE/ 105.6/ 104.5	0.39 %	0.25
0.029	MI/ 66	0.19 %	0.25, 0.5, 0.67

EXPERIMENTAL RESULTS

Small-Scale Tests

Reverse bending. The fatigue life of the lead is clearly affected by both the tests frequency and the shaper curvature. The nominal strain ranges are obtained by using the specimen thickness together with Equation 1 and the approximate the strain rate according to Equation 2:

$$\dot{\varepsilon} = 2 \cdot f[\text{Hz}] \cdot \Delta\varepsilon \quad (2)$$

The modified frequency strain life equation (Wong, 2016) is adopted where the frequency value is replaced with the estimated strain rate calculated following Eq. 2.

$$\Delta\varepsilon = A(N\dot{\varepsilon}^{-p})^\beta \quad (3)$$

where A, β and p are constants of which p dictates the strain rate dependency. Figure 3 show the results together with the best fit solution of the damage model.

A strain rate dependency (p) of 0.21 was calculated by a fitting the test data to Equation 3.

Tension-compression. Equation 3 set the basis for the construction of the fatigue curve where the strain rate component is neglected, i.e. the high strain rate curve is constructed based on the strain life equation without frequency modification. Figure 4 is a plot of the tension-compression results and corresponding fatigue curve. Selected reverse bending results from tests conducted at comparable strain rates ($\sim 0.7e^{-2}$ 1/s) are also plotted in the same graph to facilitate a direct comparison.

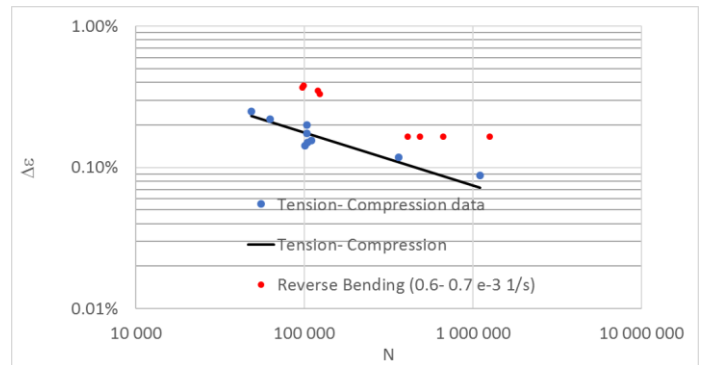


Fig. 4. Tension-compression results and calculated fatigue curve. The high strain rate reverse bending result ($0.6-0.7 e^{-2}$ 1/s) are also reported.

Full Scale Tests

MI power cables and XLPE power phases test results are shown in Figure 5 and 6. All the test results are normalized to the average strain rate for the tests according to the modified damage model identified from reverse bending results.

Fatigue $\Delta\varepsilon$ - N curves are estimated by the Maximum Likelihood Method (MLM) where the fatigue life follows a log-normal distribution. The method described in Pascual (1997), but with fixed standard deviation and introduction of a component to account for unknown point of failure is adopted in this study.

The likelihood function is described as follow:

$$L(\theta) = \prod_{i=1}^n F(X_i|\theta)^{\delta_i} R(X_i|\theta)^{1-\delta_i} \quad (4)$$

where F and R is the cumulative probability of failure and survival, respectively. δ assigned after dissection observation as follow:

$$\delta = \begin{cases} = 1, & \text{if the sample has failed} \\ = 0, & \text{if the sample has not failed} \end{cases}$$

The reliability function is given by:

$$R(X|\theta) = 1 - F(X|\theta) = 1 - 0.5 \left[1 + \operatorname{erf} \left(\frac{\ln(X_i) - \bar{X}}{\sigma\sqrt{2}} \right) \right] \quad (5)$$

Assume the fatigue life can be described according to the Coffin-Manson relation:

$$\bar{X} = \ln N = \ln A + m \ln \Delta\varepsilon \quad (6)$$

the fatigue parameters $\ln(A)$, m and standard deviation, σ are estimated by maximizing the likelihood function. To simplify the calculations:

$$\ln L(\theta) = \sum_{i=1}^n \ln(R(X_i|\theta)^{\delta_i}) \ln(1 - F(X_i|\theta)^{1-\delta_i}) \quad (7)$$

By maximizing Equation 7 through a Raphson-Newton iterative scheme, the best-fit fatigue parameters are obtained.



Fig. 5. Full scale results for MI power cables together with the results normalized to the average testing strain rate and the calculated maximum likelihood function.



Fig. 6. Full scale results for XLPE power phases together with the results normalized to the average testing strain rate and calculated the maximum likelihood function.

Post-Test Dissection Observations

The test objects were dissected after testing and any identified fracture by die-pen or visual inspection deemed the test result as failure. Tests exceeding the number of cycles given by the calculated fatigue curve tended toward an increasing severity and frequency of cracks.

The characteristics of the test object prior to- and after failure differ between MI power cable test objects and XLPE power phases. High and low strain ranges also were a discriminant in the type of observed cracks. XLPE showed a tendency to initiate cracks from pre-existing discontinuities running in a helical direction whereby the cracks mainly propagate in circumferential direction for $\Delta\varepsilon$ tests $> 1.0\%$ (reference to Figure 7). Cracks propagating along the discontinuities were also found.

The majority of XLPE power phase tested for a strain range of approximately $\Delta\varepsilon=0.4\%$, cracked following the discontinuities as shown in Fig. 8.

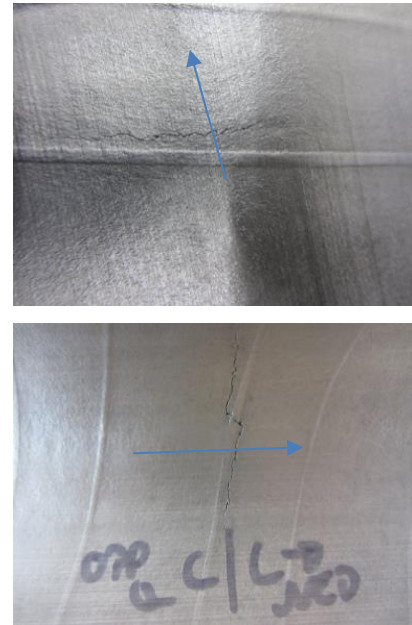


Fig. 7. (Upper) Inside of a XLPE power phase after 15,000 cycles at 1.1 % $\Delta\varepsilon$; (Lower) Inside of a XLPE power phase after 25,000 cycles. Arrow indicate axial object direction.

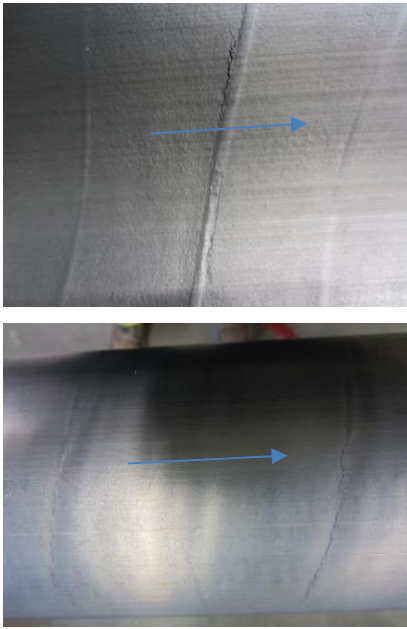


Fig. 8. (Upper) Inside of a XLPE power phase after 30,000 cycles at 0.4 % $\Delta\epsilon$; (Lower) Outside of the same test object. The blue arrow represents the axial direction.

Another distinct feature for both tested $\Delta\epsilon$ levels where deformation aligned with the same discontinuities is shown in Figure 9.



Fig. 9. (Upper Left) Outside of a (failed) XLPE power phase after 15,000 cycles at 1.1 % $\Delta\epsilon$; (Upper Right) Outside of a (run- out) XLPE power phase after 25,000 cycles at 0.4 % $\Delta\epsilon$; (Lower) Outside of a (failed) XLPE power phase after 30,000 cycles at 0.4 % $\Delta\epsilon$.

Helical discontinuities of comparable or worse severity were found also for MI power cables (Figure 10). Cracks initiated also from these, but predominantly propagated along the sheathing circumference- not the helical direction of discontinuities. This is the case for all tested $\Delta\epsilon$. The large amount of deformation observable at the cracked location evident in all the failed XLPE power cables were absent. Figure 11 show the typical failure characteristics.

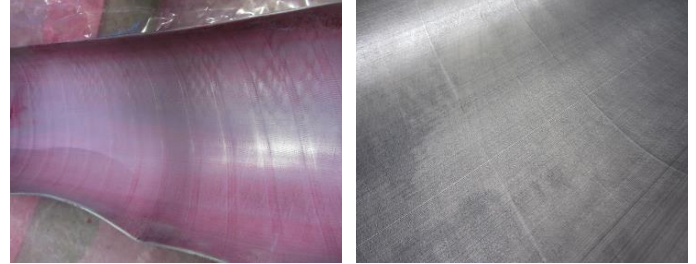


Fig. 10. (Upper Left) Inside of (run-out) MI power cable after 65,000 cycles at 1.02 % $\Delta\epsilon$; (Upper Right) Outside of a (run- out) XLPE power phase after 40,000 cycles at 0.40 % $\Delta\epsilon$;

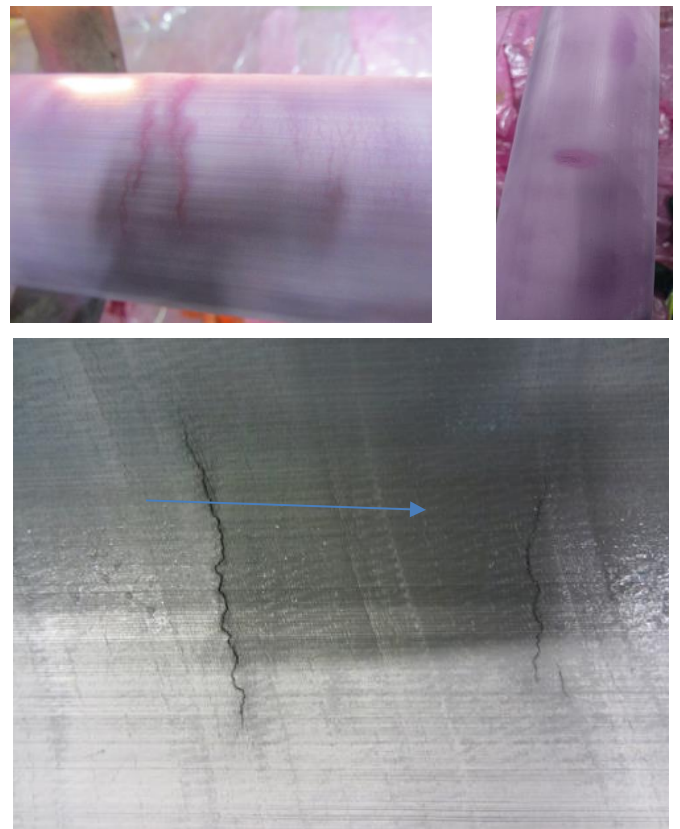


Fig. 11. (Upper Left) Outside of a (failed) MI power cable after 75,000 cycles at 1.02 % $\Delta\epsilon$; (Upper Right) Outside of a (failed) MI power cable after 60,000 cycles at 1.02 % $\Delta\epsilon$; (Lower) Inside of a (failed) MI power cable after 300,000 cycles at 0.36 % $\Delta\epsilon$. The blue arrow represents the axial direction.

CONCLUSIONS

The fatigue life of lead strongly depends on loading mode. Reverse bending of small-scale test specimen results in significantly improved fatigue life compared to tension-compression (Figure 4 and 12). Power cable subjected to bending introduce mostly tension-compression type of load on its lead sheath. Based on this it is not advisable to base fatigue calculation of tubular sheathing from reverse bending of small-scale specimens.

The fatigue life of lead is greatly enhanced when tested in a MI Power cable design compared to small-scale. The tested MI power cable designs used axial and transversal armoring which would introduce hoop stress and potentially prevent local ratcheting. The latter is supported by the post-test dissections where the ridges observed on the XLPE power phases are absent. The extension of full-scale fatigue life can also be related to modification of the hysteresis under bending where compression from the armoring elements shift the hysteresis towards compression which could modify both crack-opening, closing and potentially arrest.

Ongoing work is aimed towards understanding these mechanisms for lead alloys and cable design.

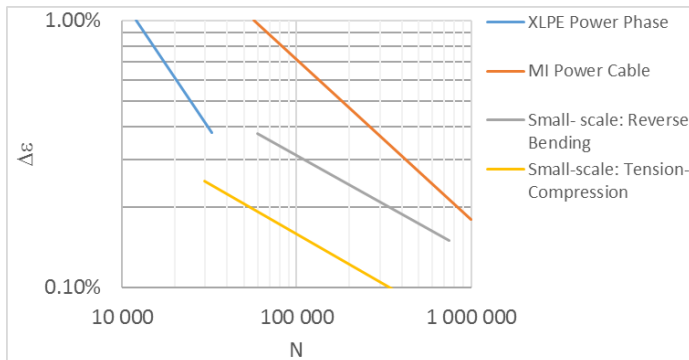


Fig. 12. Comparison of the XLPE, MI and small-scale fatigue curves. All curves are modified to a common strain rate corresponding to the average strain rate for all tests. Curves are plotted for their tested $\Delta\epsilon$ range.

The enhanced fatigue life of observed for MI power cables compared to small-scale results appears to be significantly reduced or absent for XLPE power phases. The XLPE power phase do potentially overlap with the small-scale data, but additional experiments towards the high-cycle region is required.

Over the range of strain rates investigated in full scale MI power cable testing, the strain rate dependency extracted from reverse bending fits relatively well. By increasing the strain rate sensitivity from 0.21 to 0.35, a minor improvement of fit for the MI power cables tests is observed, effectively reducing the scatter identified by the maximum likelihood method (Figure 13). This puts into question the applicability of the identified strain rate dependency for full scale results. As the strain rate sensitivity is not based on tests reflecting the correct loading mode or representing a physically meaningful description of the underlying fatigue-creep interaction, care should be taken when extrapolating the test results outside the test range.

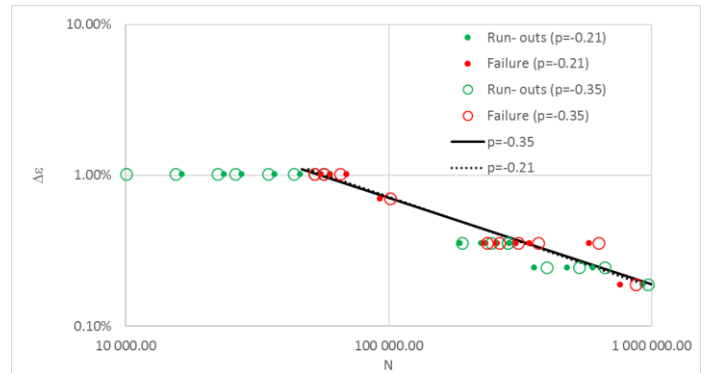


Fig. 13. The increase in strain rate sensitivity parameter (p) from 0.21 (as calculated from the small-scale experiments), to 0.35 determine a shift of the failure points below the calculated mean curve towards or above the curve. A higher strain rate sensitivity will in other words better explain the observations.

The majority of the fractures on full scale tests appear to initiate in surface discontinuities. It is clear that the identified discontinuities do affect the fatigue life, but their effect appear to be different for MI and XLPE power cables. For XLPE cables the fractures locations are often associated with local deformation in the form of ridges intimate to the fracture location. The same observation is not made for neither reverse bending or tension-compression small-scale tests even if the fatigue life were similar. This could indicate that the apparent negative effect from discontinuities on the sheathing is offset by other positive effects such as the absence of an edge on tubular sheathing. This statement is supported by a previous study, which demonstrates a low influence of severe stress concentrators on the fatigue life of lead (Johanson et al., 2018).

ACKNOWLEDGEMENTS

This work has been financed by Nexans Norway and the Research Council of Norway through ENERGIX Programme, Contract No. 256367/E20.

REFERENCES

- E.H. Wong, W. v. (2016). Creep fatigue models of solder joints: A critical review. *Microelectronics Reliability*, 1-12.
- Johanson, A., Viespoli, L., Nyhus, B., Alvaro, A., & Berto, F. (2018). Experimental and numerical investigation of strain distribution of notched lead fatigue test specimen. *12th International Fatigue Congress*. Poitiers.
- P.Anelli, F. (1986). The Fatigue Life of Lead Alloy E as a Sheathing Material for Submarine Power Cables.
- Pascual, F. (1997). Analysis of Fatigue Data with Runouts Based on a model with Non- constant Standard Deviation and a Fatigue limit parameter. *Journal of testing and evaluation*, 25(3), 292- 301.
- Viespoli, L., Johanson, A., Alvaro, A., Nyhus, B., Sommacal, A., & Berto, F. (2019). Tensile characterization of a lead alloy: creep induced strain rate sensitivity. *Materials Science & Engineering A*, 744, 365-375.